Supporting Information

Li et al. 10.1073/pnas.1505649112

SI Materials and Methods

Genetically Modified Mice. *Adam17*$^{-/-}$ mice (*A17*$^{-/-}$) and *iRhom2*$^{-/-}$ mice (*iR2*$^{-/-}$) have been described previously (1, 2) and were of mixed genetic background (129Sv,C57BL/6). *iRhom1*$^{-/-}$ mice (*iR1*$^{-/-}$) were generated from a conditionally targeted C57BL/6N ES cell line obtained from the European Conditional Mouse Mutagenesis Program (EPD0577_2_H04; the parental cell line was JM8A3.N1, derived from JM8 cells, which in turn were isolated from C57BL/6N mice carrying a targeted repair of the C57BL/6 nonagouti mutation). The targeted allele contains loxP sites upstream of *iRhom1* exon 4 and downstream of *iRhom1* exon 11. Chimeric mice were generated by injection of targeted ES cells into blastocysts from C57BL/6 mice. Matings of these chimeric mice with C57BL/6 wild-type mice produced heterozygous offspring carrying the targeted *iRhom1* allele in the germ line (referred to as *iRhom1t*/+). *iRhom1t*/+ mice were mated with FVB/*N-Tg*(*EIIa-cre*)*C5379Lmgd*/*J* transgenic mice (referred to as *EIIa-Cre*) (3) to remove the neo selection marker together with exons 4–11 (see Fig. 1*A* for details). The resulting allele contains exons 1–3 that splice onto the Engrailed 2 (E2) splice acceptor site, which is followed by the E2 exon, an internal ribosomal entry site (IRES), a LacZ gene, and a polyadenylation site. The ATG codon for iRhom1 is in exon 2, so amino acid residues 1–82 are encoded by this mRNA, followed by a stop codon. The poly(A) site after the LacZ gene will terminate transcription, thus ensuring that none of the remaining parts of iRhom1 that are encoded by exons 12–18 can be synthesized. These animals, referred to as *iR1*$^{+/-}$ mice, were mated with one another to generate *iR1*$^{-/-}$ mice (C57BL/6N,FVB genetic background). In all experiments with *iR1*$^{-/-}$ mice, wild-type littermates served as control. To generate mice lacking iRhoms 1 and 2, *iR1*$^{-/-}$ mice were crossed with *iR2*$^{-/-}$ mice (2) (129Sv,C57BL/6) and, after backcrossing with *iR2*$^{-/-}$ mice, those animals that lacked *iRhom2* and had one mutant allele of *iR1* (*iR1*$^{+/-}$*2*$^{-/-}$) were kept and mated with one another. These matings yielded *iR1*/*2*$^{-/-}$ double knockout offspring at the expected Mendelian ratio (Fig. S3). All *iR1*/*2*$^{-/-}$ double knockout mice were of mixed genetic background (129Sv, C57BL/6N,FVB). All animal experiments were approved by the Internal Animal Use and Care Committee of the Hospital for Special Surgery.

Western Blot Analysis. For Western blots of the pro- and mature forms of ADAM17 in different tissues of adult *iRhom1*$^{-/-}$ mice and wild-type controls, the heart, liver, lung, spleen, kidney, brain, or different areas of the brain were isolated and processed as previously described (4), and the same approach was used to prepare samples for Western blots of different tissues in newborn mice (P1). The mEFs used for Western blot analysis were lysed on ice in Tris-buffered saline (TBS) with 1% Triton X-100, 1,10-phenantroline (10 mM), and protease inhibitor mixture (Roche Applied Science). Phosphatase inhibitors (5 μM NaF, 2 μM vanadate, 0.25% Na deoxycholate) were added to the lysis buffer for samples that were subjected to Western blot analysis with antibodies against pEGFR. Cell lysates were centrifuged at 4 °C for 15 min at 16,110 × *g* to remove nuclei and cell debris, and the cleared supernatants were then incubated with 40 μL ConA Sepharose CL4B (GE Healthcare) for 2 h at 4 °C. Bound glycoproteins were eluted in SDS loading buffer with 2% β-mercaptoethanol for 10 min at 95 °C. Comparable amounts of protein were loaded on 10% acrylamide gels and transferred to nitrocellulose membranes (Pall), which were blocked in 5% nonfat milk and then incubated in primary antibody for 1 h, washed three times in TBS, 0.5% Tween 20, and incubated in HRP-labeled donkey anti-rabbit secondary antibody. Bound antibodies were detected using the ECL system (Amersham Biosciences) and a ChemiDoc image analyzer (Bio-Rad), and the images were assembled using Microsoft PowerPoint software. Loading controls were generated by stripping membranes for 30 min at 55 °C in stripping buffer (2% SDS, 50 mM β-mercaptoethanol in 62 mM Tris, pH 6.7) followed by incubation with anti-ADAM9 antibodies. The rabbit antibodies against the cytoplasmic domain of ADAM9 or ADAM17 have been previously described (5, 6).

Quantitative PCR Analysis. Total RNA was extracted from heart, liver, lung, spleen, kidney, and brain using the RNeasy Mini Kit (Qiagen). RNA was reverse-transcribed by M-MuLV Reverse Transcriptase (New England BioLabs). qPCR (SYBR Green; ABI PRISM 7900HT; Applied Biosystems) was normalized to GAPDH. The following primers were used for the qPCR analysis: iR1 exon 1/2 primers and mouse GAPDH primers were from Qiagen. Other exon primers were from Gene Link: iR1 exon 4/5 forward: 5′-GCTAAAGCCGCAGGTCATCC-3′; iR1 exon 4/5 reverse: 5′-GTCATCAGCCATGCGAAAGG-3′; iR1 exon 12/13 forward: 5′-CCAGACCTTGCAGGCAACAAG-3′; iR1 exon 12/13 reverse: 5′-CGGCCACTTGGTGATATCTTC-3′; iR1 exon 16/17 forward: 5′-GTGCACTGCATGGACGATGTC-3′; iR1 exon 16/17 reverse: 5′-GACCGTCATCTGGAAGCAGAC-3′.

Histopathological Analysis. Following euthanasia of 13.5-wk-old *iR1*$^{-/-}$ and wild-type mice (two of each genotype) by carbon dioxide (according to the guidelines of the American Veterinary Medical Association), all organs were examined grossly and fixed in 10% neutral buffered formalin or 4% paraformaldehyde. Tissues were processed routinely for histology and embedded in paraffin, sectioned at 4-μm thickness, stained with hematoxylin and eosin, and examined. The following tissues were examined: semimembranosus and semitendinosus muscles, sciatic nerve, heart, blood vessels, thymus, lungs, kidneys, salivary glands, lymph nodes (submandibular, mesenteric), stomach, duodenum, jejunum, ileum, cecum, colon, pancreas, thyroid gland, esophagus, trachea, adrenal glands, liver, gallbladder, spleen, uterus, ovaries, urinary bladder, skin (trunk, head), femur, tibia, stifle joint, humerus, sternum, bone marrow), brain, pituitary gland, ears, eyes, nose, mouth, teeth, vertebrae, intervertebral discs, and spinal cord. Finally, the brains were stained with Luxol fast blue for myelin. This analysis did not uncover any evident histopathological defects in *iR1*$^{-/-}$ mice compared with their wild-type control littermates. The histopathological analysis of newborn *iR1*$^{-/-}$, *iR2*$^{-/-}$, *iR1*/*2*$^{-/-}$, and *A17*$^{-/-}$ and wild-type control mice (at least three mice per genotype) was performed after euthanasia by carbon dioxide for 5 min followed by decapitation on tissues fixed in 10% neutral buffered formalin. The following tissues were analyzed: heart, with an emphasis on the aortic, pulmonic, and atrioventricular valves; bones, with an emphasis on the femoral and humeral growth plates; and eyes, skin, skeletal muscle, joints, bone marrow, spinal cord, lung, thymus, kidneys, adrenal glands, liver, spleen, pancreas, esophagus, stomach, small intestine, large intestine, blood vessels, nasal cavity, oral cavity, and teeth. Aside from the defects in eyelid closure, the thickened semilunar heart valves, and the enlarged zone of hypertrophic cells in the growth plate of the femur and humerus of *iR1*/*2*$^{-/-}$ and *A17*$^{-/-}$ mice, no histopathological abnormalities were observed in the newborn mice of different genotypes analyzed for this study.

The histomorphometry of the newborn heart valves was performed on sections of valve leaflets of aortic, pulmonic, tricuspid, and mitral valves of hearts of three newborn mice (P1) per genotype, for a total of 15 hearts. For this purpose, we isolated hearts from newborn wild-type or mutant mice, fixed them in 10% neutral buffered formalin, and generated serial paraffin sections of 5-μm thickness oriented in the long axis of the heart, of which every third section was mounted on a slide, stained with hematoxylin and eosin, and coverslipped. Each mounted section was then photographed using a Nikon Eclipse 50i equipped with a Nikon Digital Sight DS-5M camera, and images were acquired with NIS-Elements version 4.0 software. An equivalent section of each of the four valves for three hearts per genotype was selected for histomorphometry. For the selection process, we identified all sections in a heart that contained parts of a given valve, and then selected the section providing a view of the most elongated aspect of that particular valve leaflet for each genotype. For quantification, we measured the length of the leaflet and the overall surface area using ImageJ Windows version 1.48 (NIH), and calculated the average width of the selected valve leaflet by dividing the area by the length for each of the three newborn mice per genotype and per valve. The average and SD of these numbers were calculated using Microsoft Excel, and the statistical significance of any changes compared with the wild-type valves was assessed using the Student's *t* test. A P value of <0.05 was considered significant.

Generation of Mouse Embryonic Fibroblasts. Embryonic fibroblasts were isolated from E13.5 *iR1*$^{-/-}$ and *iR1/2*$^{-/-}$ embryos to generate primary mEFs for immortalization as previously described (7). Briefly, the head and viscera of E13.5 embryos were removed and the remaining tissue was minced and then trypsinized in 0.25% trypsin for 15 min at 37 °C. Cells were released through mechanical trituration and grown in Dulbecco's modified Eagle medium supplemented with antibiotics and 10% FCS. Primary mEF cells were immortalized by transfection with a plasmid carrying the simian virus 40 (SV40) large T antigen.

1. Horiuchi K, et al. (2007) Cutting edge: TNF-alpha-converting enzyme (TACE/ADAM17) inactivation in mouse myeloid cells prevents lethality from endotoxin shock. *J Immunol* 179(5):2686–2689.
2. McIlwain DR, et al. (2012) iRhom2 regulation of TACE controls TNF-mediated protection against *Listeria* and responses to LPS. *Science* 335(6065):229–232.
3. Lakso M, et al. (1996) Efficient in vivo manipulation of mouse genomic sequences at the zygote stage. *Proc Natl Acad Sci USA* 93(12):5860–5865.
4. Issuree PD, et al. (2013) iRHOM2 is a critical pathogenic mediator of inflammatory arthritis. *J Clin Invest* 123(2):928–932.
5. Weskamp G, Krätzschmar J, Reid MS, Blobel CP (1996) MDC9, a widely expressed cellular disintegrin containing cytoplasmic SH3 ligand domains. *J Cell Biol* 132(4):717–726.
6. Schlöndorff J, Becherer JD, Blobel CP (2000) Intracellular maturation and localization of the tumour necrosis factor alpha convertase (TACE). *Biochem J* 347(Pt 1):131–138.
7. Sahin U, et al. (2006) A sensitive method to monitor ectodomain shedding of ligands of the epidermal growth factor receptor. *Epidermal Growth Factor: Methods and Protocols, Methods in Molecular Biology*, eds Patel TB, Bertics PJ (Humana, Totowa, NJ), Vol 327, pp 99–113.

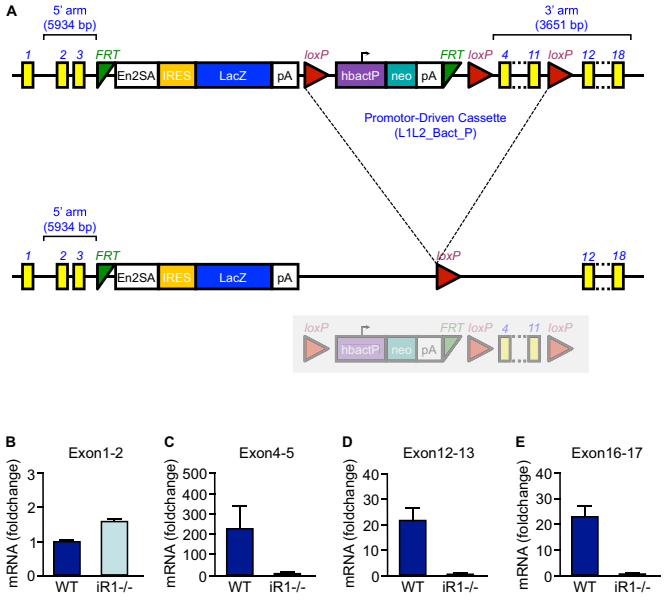

Fig. S1. Diagram of the iR1 targeting construct and qPCR analysis of the expression of different exons of iR1 in *iR1*$^{-/-}$ mice. (*A*, *Top*) Schematic of the targeting construct for *iR1*$^{-/-}$ mice (modified with permission from the International Mouse Phenotyping Consortium). The first three exons of iR1, which encode the N-terminal 82 amino acid residues of iR1 in exons 2 and 3, are followed by a flippase recombination target (FRT) site, an Engrailed 2 splice acceptor site (En2SA), an IRES, and a LacZ gene, which is flanked by a polyadenylation (pA) site. Following the pA site is a loxP site, an hbact promoter driving expression of the neo selection marker, which is flanked by a pA site followed by an FRT site. The next segment contains exons 4–11, which are flanked by loxP sites, followed by exons 12–18. The animals used in this study were generated by crossing mice carrying the targeted allele with mice expressing the Cre transgene under control of the EIIa promoter, which is expressed in the germ line. This leads to the excision indicated, removing exons 4–11. Because of the pA site next to the LacZ gene, the expression of exons 1–2 can be detected by qPCR, whereas exons 4–5, 12–13, and 16–17 are not expressed, as evidenced by the lack of the qPCR signal generated with primers that amplify sequences in these exons in wild-type controls (*B*–*E*). Error bars: ±SD.

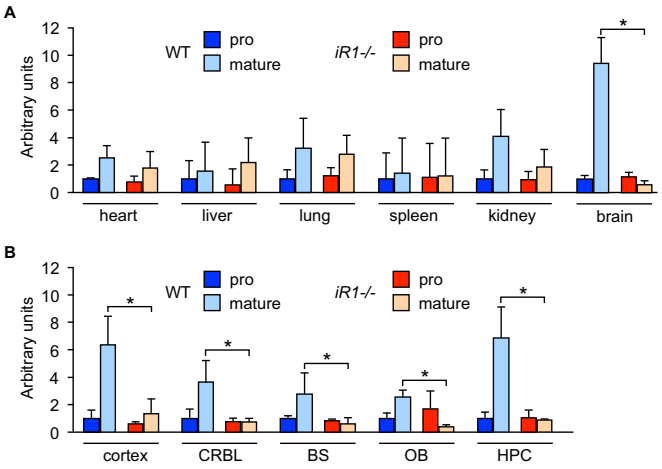

Fig. S2. Densitometric quantification of pro- and mature ADAM17 in the tissue Western blots shown in Fig. 2. (*A*) Densitometric quantification of three Western blots prepared from separately isolated tissues from three *iR1*$^{-/-}$ mice and wild-type controls corroborates that the expression of mature ADAM17 is abolished in the brain of *iR1*$^{-/-}$ mice but is comparable to wild-type mice in other tissues. (*B*) Quantification of pro- and mature ADAM17 in different brain areas shows that mature ADAM17 is strongly reduced in the cortex, cerebellum (CRBL), brainstem (BS), olfactory bulb (OB), and hippocampus (HPC) of *iR1*$^{-/-}$ mice compared with wild-type controls. **P* < 0.05; ±SD (*n* = 3).

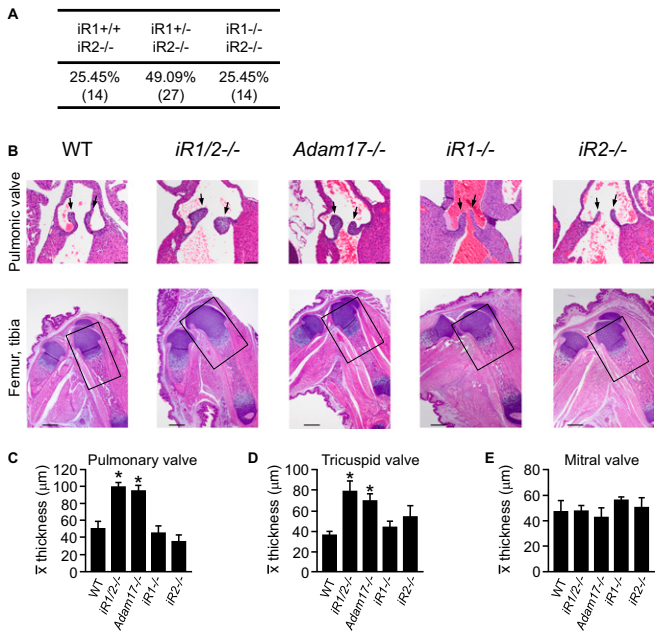

Fig. S3. Table of offspring of matings of *iR1*$^{+/-}$*iR2*$^{-/-}$ mice and analysis of the pulmonic valve and growth plate in newborn mice. (*A*) The offspring from matings of mice lacking iR2 that were also heterozygous for iR1 followed the expected Mendelian distribution for mice with no lethality during embryonic development. (*B*) Sections of the pulmonic valve and low-magnification images of the growth plates of the femur and tibia of newborn wild-type, *iR1/2*$^{-/-}$, *Adam17*$^{-/-}$, *iR1*$^{-/-}$, and *iR2*$^{-/-}$ mice. Arrows point to the pulmonic valve leaflets, which are thickened in relationship to their length in newborn *iR1/2*$^{-/-}$ and *Adam17*$^{-/-}$ mice when compared with wild-type controls, whereas the pulmonic valve leaflets in *iR1*$^{-/-}$ and *iR2*$^{-/-}$ mice resemble wild-type controls. The boxes around the femur indicate the position of the sections shown in Fig. 4. [Scale bars, 100 μm (*B*, *Top*) and 500 μm (*B*, *Bottom*).] (*C*–*E*) Quantification of the surface area divided by the length of individual valve leaflets of the pulmonary valve (*C*), tricuspid valve (*D*), and mitral valve (*E*) (see *SI Materials and Methods* for details). $\bar{x}$, average. **P* < 0.05; ±SD (*n* = 3).

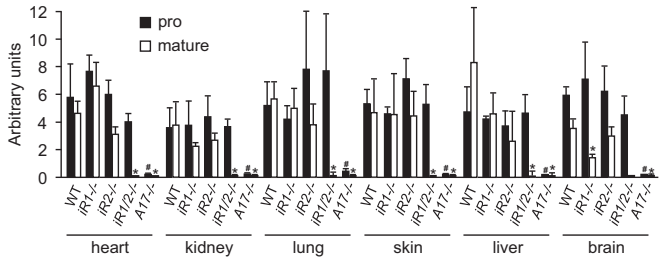

Fig. S4. Densitometry of pro- and mature ADAM17 in the tissue Western blots shown in Fig. 5. Both pro- and mature ADAM17 are absent in all *A17*$^{-/-}$ tissues examined, whereas only mature ADAM17 is abolished in tissues from *iR1/2*$^{-/-}$ mice. The relative amounts of pro-ADAM17 in *iR1/2*$^{-/-}$, *iR1*$^{-/-}$, *iR2*$^{-/-}$, and wild-type mice are comparable. The asterisk indicates a significant reduction in the mature form of ADAM17 compared with wild-type controls. # indicates a significant reduction in pro-ADAM17 compared with wild-type controls. $P < 0.05$; ±SD ($n = 3$).

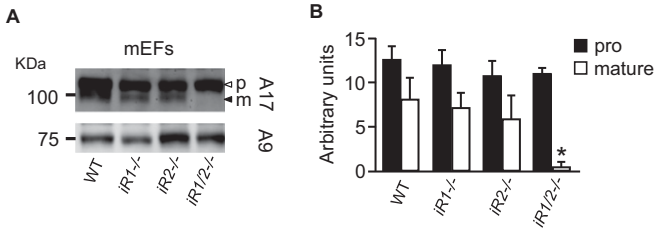

Fig. S5. Analysis of ADAM17 maturation by Western blot in wild-type (WT) *iR1*$^{-/-}$, *iR2*$^{-/-}$, *or iR1/2*$^{-/-}$ mEFs. *iR1*$^{-/-}$ or *iR2*$^{-/-}$ mEFs have similar levels of mature ADAM17 as wild-type controls, whereas *iR1/2*$^{-/-}$ double knockout mEFs have no detectable mature ADAM17 (*A*) (quantification of three blots is shown in *B*). *$P <$ 0.05; ±SD ($n = 3$).

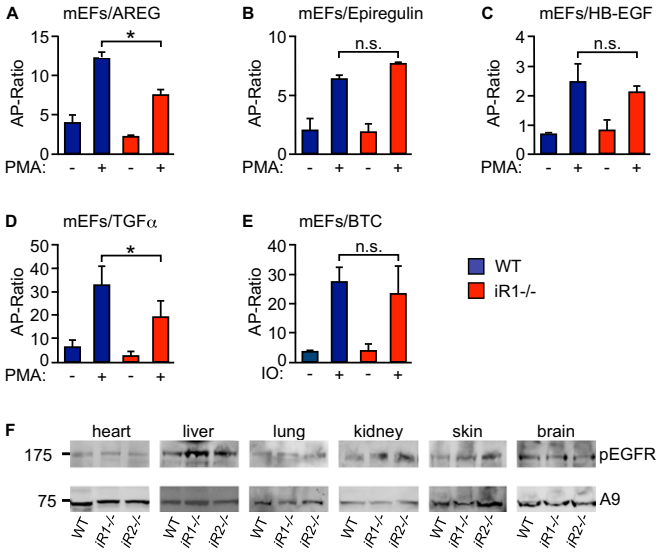

Fig. S6. Shedding of EGFR ligands from *iR1*$^{-/-}$ mouse embryonic fibroblasts or wild-type controls and Western blot of EGFR phosphorylation in different tissues of wild-type (WT) *iR1*$^{-/-}$ and *iR2*$^{-/-}$ mice. PMA could stimulate the shedding of alkaline phosphatase-tagged amphiregulin (*A*), epiregulin (*B*), HB-EGF (*C*), and TGF-α (*D*) in embryonic fibroblasts isolated from *iR1*$^{-/-}$ mice, although the PMA-stimulated shedding of amphiregulin and TGF-α was reduced compared with controls. The ionomycin-stimulated shedding of the ADAM10 substrate betacellulin (BTC) was comparable in *iR1*$^{-/-}$ mEFs and wild-type controls (*E*). Western blot analysis of phosphorylated EGFR in different tissues of newborn *iR1*$^{-/-}$ or *iR2*$^{-/-}$ mice shows similar EGFR phosphorylation in extracts of heart, liver, lung, kidney, skin, and brain compared with newborn wild-type controls (*F*). *$P < 0.05$; ±SD ($n = 3$).